Predictions of settlement risk induced by tunnelling using BIM and 3D visualization tools

Providakis, Stylianos; Rogers, Chris; Chapman, David

DOI:
10.1016/j.tust.2019.103049

Document Version
Peer reviewed version

Citation for published version (Harvard):
Providakis, S, Rogers, C & Chapman, D 2019, 'Predictions of settlement risk induced by tunnelling using BIM and 3D visualization tools', *Tunnelling and Underground Space Technology*, vol. 92, 103049. https://doi.org/10.1016/j.tust.2019.103049

Predictions of settlement risk induced by tunnelling using BIM and 3D visualization tools

Stylianos Providakis, Chris D.F. Rogers and David N. Chapman*

Department of Civil Engineering, University of Birmingham, Birmingham B15 2TT, UK

Abstract

Ground settlements caused by tunnelling excavations are particularly important in urban areas, with greater relevance in soft soils. Estimating the settlement risk to adjacent buildings is an important consideration for tunnel planning, design and construction. In recent years the need to extend the Building Information Modelling (BIM) concept to the subsurface of modern urban areas has been increasingly emphasized, with the aim of providing better geotechnical data management and making three-dimensional (3D) data visualization more understandable. This need becomes imperative in cases of tunnelling excavations.

This paper presents a newly-developed methodology to utilize 3D-BIM based models, with the associated geological information, to analyse three-dimensional models for the prediction of the tunnelling-induced settlement damage susceptibility of buildings. The engineering parameter information associated with settlement risk factors is extracted from a BIM file of a specific building project, employing the IFC standard to act as a bridge between the BIM data and MATLAB meshing and analysis tools for the evaluation of tunnel safety risks. Particular features of the methodology are that the buildings are modelled together with the ground, the subsurface geology and the representation of the tunnel, and all of them in 3D. This methodology has made use of a combination of MATLAB tools, the 3D visualization capabilities of the Sketchup design software and the conversion procedures from BIM to IFC to STL models and vice versa.

As a result, the developed automated settlement susceptibility checking-platform informs tunnel construction engineers and managers by reporting, why, where and when settlement might occur, and

*Corresponding author: S. Providakis, email: SXP621@student.bham.ac.uk.

Prof. C. Rogers, email: c.d.f.rogers@bham.ac.uk. Prof. D. Chapman, email: d.n.chapman@bham.ac.uk.

what safety measures are needed for preventing settlement-related accidents before construction starts. An example case study of such a system is provided to illustrate the methodology, and thereby demonstrates both that adjustments to the location (alignment) of the tunnel can have a major impact on the risk of settlement-related damage.

Keywords

Settlement risk prediction, underground-BIM, building damage assessment, 3D ground model, 3D building-tunnel interaction

1. Introduction

Due to the continuing expansion of cities, understanding ground-related hazards is of importance to ensure urban safety and a sustainable future, and hence this should be clearly adopted in related planning and decision-making as indicated by Price et al. (2016).

One such ground related hazard (geohazard) that should be accounted for is ground settlement and is investigated in the present paper. Ground settlement is related to the use of urban underground space, and the importance of this in aligning with future sustainable developments in large cities (Rogers, 2009; Hunt et al., 2016). This means that underground construction such as tunnels should be designed with respect to the relative settlement risk they pose to adjacent buildings and the consequent possible damage (Burland et al., 2001; Schindler et al., 2016). Hence, an adequate tunnelling-induced settlement risk assessment is needed. This should be carried out using specific analysis methods that could clearly indicate the risk.

There is a huge body of literature related to estimating the ground displacements caused by tunnel construction. However, for the purposes of this paper to illustrate the approaches being proposed, the empirical methodologies are discussed here, and these have been proven to be suitable for making preliminary estimations of the associated engineering interactions (Rankin, 1988 and Chapman, 2010). In

the cross-section perpendicular to the tunnel advance, the corresponding settlement trough has been shown to be approximated by a “gaussian-like” or “bell-shaped” curve with the highest settlement being directly above the tunnel’s centreline. This was adapted initially from the empirical functions by Peck (1969) and later evolved by Attewell and Woodman (1982), O’Reilly and New (1982), Attewell et al. (1986) and Mair et al. (1996). Accounting for more factors led to analytical methods with more sophisticated equations, such as those produced by Sagaseta (1987) and Verruijt and Booker (1996). In the same context, Loganathan and Poulos (1998) considered the corresponding ground-loss deformations that take place. Thus, the settlement trough used in these approaches could efficiently provide the tunnelling-induced settlement susceptibility in combination with the integrated 3D visualizations of the ground-building interactions.

One of the key results of the ground displacements caused by tunnel construction is the effect on adjacent buildings. The damage can be shown to be related to both the position of the structure in relation to the ground settlement trough and the relative structural deformation (Burland and Wroth, 1974; Burland et al., 1977; Attewell et al., 1986). Burland and Wroth (1974) and Burland et al. (1977) assumed the building to be a simple beam and adopted the risk of damage in terms of critical strain (later called the Limited Tensile Strain method). Moreover, specific criteria related to the structural damage and critical strain have been adapted by Boscardin and Cording (1989), Burland (1995), Mair et al. (1996) to provide a thorough categorization of the building-related risk. These can be integrated with the corresponding ground settlement and slope indicators proposed by Rankin (1988). Thus, these damage criteria provide a clear preliminary assessment for indicating the tunnelling-induced risk to adjacent structures. However, if these criteria could be visualized multidimensionally they could provide an integrated assessment method and could align with other recent urban geohazard modelling research.

Building Information Modelling (BIM) is an emerging design technology that overcomes these limitations by storing, sharing and multidimensionally visualizing all the information regarding all the structural characteristics for all the stages during the lifecycle of a building (Eastman et al., 2011). This

platform is mainly adopted for structural design aspects, but there is potential to include geotechnical information (Kessler et al., 2015; Tawelian and Mickovski, 2016). Borrmann et al. (2014) and Kim et al. (2015) incorporated the database advantages of BIM to underground applications. It is evident there is a gap in relation to an integrated geohazard assessment tool utilising the entire capability of BIM in terms of its database and 3D visualization, but one that aligns with the recent construction and geotechnical research.

In terms of the database advantages of BIM this is mainly due to the open Industry Foundation Classes (IFC) format (buildingSMART, 2017), which is widely accepted and used in construction-industry-BIM (Steel et al., 2012). In addition to the previous database aspects, another format that allows 3D objects to be represented and transferred between several different pieces of software is the "STereoLithography" or STL format adopted by 3D systems (2018). This is widely used for 3D object data modification and mesh transfer (Kumar and Dutta, 1997; Chiu and Tan (2000); Qu and Stucker, 2003). Furthermore, an integration of this format with BIM to provide a platform to transfer the mesh, supporting BIM, would be appropriate for assessment analyses involving many parameters, such as the case of the urban geohazard risk.

The present study utilises the settlement trough approach and the analytical methodology proposed by Loganathan and Poulos (1998) to provide the tunnelling-induced urban ground settlement susceptibility of adjacent buildings as a demonstrator for an integrated 3D visualization tool. These visualisations are provided in a BIM framework, adapting it to geotechnical and geological aspects and taking advantage of its database capacity. This introduces a geotechnical application to the formats that BIM supports to achieve the data exchange between the different frameworks and hence, to conduct the settlement risk assessment visually.

The paper therefore briefly introduces the approach for estimating the tunnelling-induced ground settlement, following which the BIM and IFC integration aspects are then introduced. This involves the

IFC and STL format arrangements in combination with the georeferencing that was required to provide the 3D subsurface and tunnel models and their visualization within the BIM framework. The building risk assessment is then integrated into the 3D visualisations to indicate the tunnel-building-ground interactions. The paper concludes by discussing the application of the study beyond the present demonstrator and its potential impact.

2. Previous studies for estimating the ground movements due to tunnelling excavations

The previous studies for the estimation of the tunnelling-induced ground displacements can be categorized as empirical, analytical and numerical methods and their estimations are dependent on the available database.

2.1. Empirical methods

Nowadays, the broadly used empirical methods are mainly utilized for the prediction of the surface settlements for soft ground. These methods were first introduced by Peck (1969) after a series of related in-situ observations and records, producing the corresponding "settlement trough" curve presented in Figure 1 from the Equation (1):

$$S = S_{max} \cdot \exp(\frac{-x^2}{2i^2}) \quad (1)$$

where *S* describes the transverse settlement in distance x from tunnel's centerline; *Smax* describes the max settlement at x=0, with values according to ground conditions and *i* describes the location of maximum settlement gradient (according to the ground conditions).

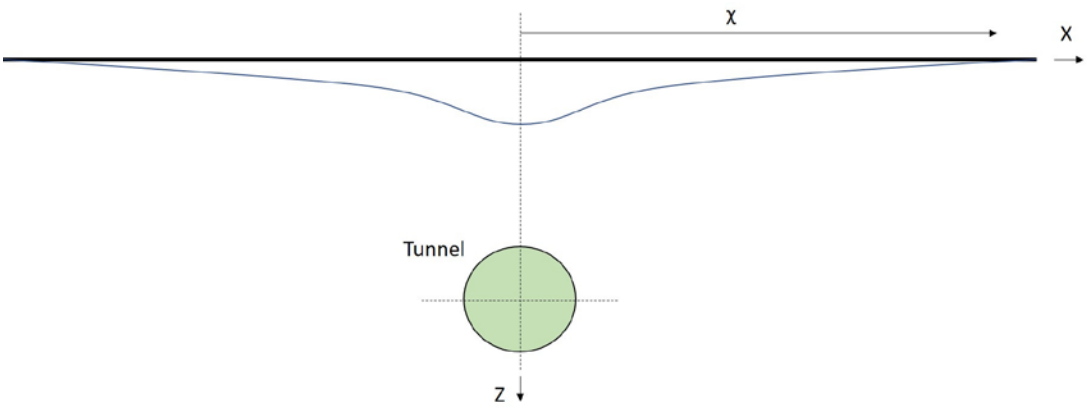

Figure 1. The settlement trough and the related ground movements, adapted from Peck (1969), O'Reilly and New (1982) Attewell et al. (1986) and Mair et al. (1996).

The next Equation (2) adapted by Mair (1993), predicts the maximum settlement from tunnelling, involving geometrical parameters important for those estimations:

$$S_{max} = \frac{0.313 V_L D^2}{i} \qquad (2)$$

where V_L is the ground volume loss (ratio of ground loss volume/tunnel volume per metre length), D is the tunnel's diameter and i describes the location of maximum settlement gradient (-values according in relation to ground conditions).

Furthermore, although empirical approaches are reasonably used for the tunnelling-induced ground settlements, they indicate some disadvantages that should be considered carefully in similar modelling (Chapman, 2010). Hence, they reveal issues of significance (Rankin, 1988) concerning:

- The inability to predict accurately the subsurface settlements and horizontal movements.
- Their adjustment to the diversity of ground conditions.

2.2. Analytical methods

The ground movements from tunnelling with respect to strains in a homogeneous, isotropic and incompressible soil from surficial ground loss is analytically studied by Sagaseta (1987). Another example of the small number of similar studies regarding the involved ground movement factors is provided by Verruijt and Booker (1996), who pointed out the same approach for a homogeneous elastic soil by utilizing the same method as Sagaseta (1987).

Verruijt and Booker (1996) also improved predictions by including Poisson's ratio for the ground loss as well as adding the impact from an oval-shaped deformation along the tunnel's centreline. The related closed-form settlement Equation (3) is provided (Verruijt and Booker, 1996), yielding the following ground settlement estimations:

$$U_z = -\varepsilon R^2\left(\frac{z_1}{r_1^2}+\frac{z_2}{r_2^2}\right)+\delta R^2\left(\frac{z_1(kx^2-z_1^2)}{r_1^4}+\frac{z_2(kx^2-z_2^2)}{r_2^4}\right)+$$

$$+\frac{2\varepsilon R^2}{m}\left(\frac{(m+1)z_2}{r_2^2}+\frac{mz(x^2-z_2^2)}{r_2^4}\right)-2\delta R^2 h\left(\frac{x^2-z_2^2}{r_2^4}+\frac{m}{m+1}\frac{2zz_2(3x^2-z_2^2)}{r_2^6}\right) \qquad (3)$$

where e is the uniform radial ground loss; δ is the long term ground deformation due to the ovalization of the tunnel lining; $z_1 = z\text{-}h$; $z_2 = x+h$; $r_1^2 = x^2+z_1^2$; $r_2^2 = x^2+z_2^2$; R is the tunnel radius; h is the depth; $m = 1(1\text{-}2v)$; $k = v/(1\text{-}v)$ and v is the Poisson's ratio of soil.

The previous equations were refined by Loganathan and Poulos (1998), who specified boundary conditions accounting for the ground loss while tunnelling. The Equation (4) by Loganathan and Poulos (1998), which models successfully the ground settlement from tunnelling excavations and leads to efficient findings, is mentioned next.

Surface Settlement

$$U_{z=0} = \varepsilon_0 R^2 \frac{4H(1-\nu)}{H^2+x^2} exp\left\{-\frac{1.38x^2}{(Hcot\beta+R^2)^2}\right\} \qquad (4)$$

where $U_{z=0}$ is the ground surface settlement, U_z is the subsurface settlement, U_x is the lateral soil movement, R is the tunnel radius, z is the depth below ground surface, H is the depth of tunnel axis level, ν is the Poisson's ratio of soil, ε_0 is the average ground loss ratio (not a displacement), x is the lateral distance from tunnel centerline and β is the Limit angle of 45 + φ/2.

3. Methodology

The previous analytical Equations (3) and (4) have been merged with the BIM-based data of buildings to generate a fully integrated and automated platform to analyze and visualize in three dimensions the tunnelling-induced settlement damage prediction and distributions to the adjacent buildings. An overview of the proposed methodology is presented in Figure 2.

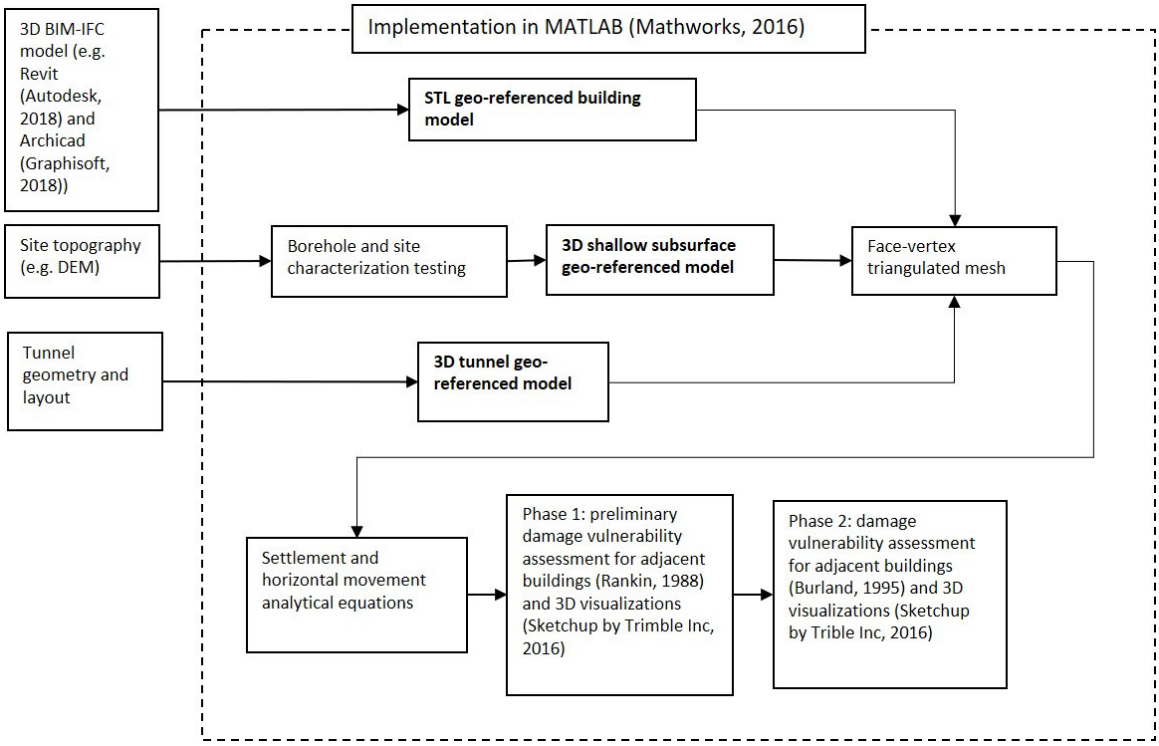

Figure 2. Proposed methodology flow chart.

3.1. 3D BIM – IFC modelling

The proposed methodology employs the IFC (buildingSMART, 2017) data standards to enable the desired building geometry and structural features and characteristics to be imported to (and exported from) BIM. This is significant for this study as it can support the integration aspects, producing the initial 3D geo-visualisations and basic features needed for the building-settlement risk assessments.

SketchUp™ by Trimble Inc. (2016) is utilized in the proposed methodology as the 3D visualization software, having an easy-to-use Graphical User Interface (GUI) while simultaneously enabling the user to easily import BIM-IFC models and further modify them in 3D.

In this study, a 3D object-based model of a two-storey building is utilized that is freely available from SUplugins (SUPodium, 2018), aligning with the BIM and IFC paradigms. The floor plan of the IFC model was developed in Archicad (Graphisoft, 2018) and Figure 3 shows the model after it has been imported in SketchUp (Trimble Inc., 2016).

The building consists of four structural-elements groups:

- 19 column objects.
- 10 beam objects.
- 22 wall objects.
- 14 slab objects.

To simulate a typical urban neighbourhood, the building was copied into ten similar buildings of different sizes as shown in 3D in Figure 4.

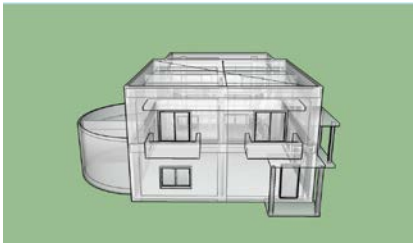

Figure 3. Original 3D IFC building model in SketchUp.

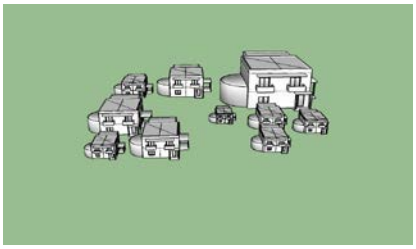

Figure 4. 3D IFC building block model in SketchUp.

This IFC-model file containing the ten buildings has been assumed to be overlaid onto a satellite image of the southwestern part of the campus of the University of Birmingham, UK as shown in Figure 5.

Figure 5. Ten IFC buildings superimposed onto the satellite image of the University of Birmingham, UK campus.

3.2. STL-georeferenced building model

In the proposed methodology, the IFC-model file previously imported into the BIM visualisation software (SketchUp), is converted at this time into the STL format. This is done in SketchUp (Trimble Inc., 2016) using its BIM capabilities, in order to allow every aspect involved to be further analysed or modelled and modified, i.e. by exporting it to MATLAB™ by Mathworks (2016) in this study. Through this format it is capable of further modifications and adjustments since it fully supports 3D characteristics including the mesh of the buildings. This is of significance for geohazard assessments, as the relative information is embedded in the corresponding mesh, to form the risk analysis.

An issue that has to be considered to handle the successful integration of BIM (-IFC) with settlement risk assessments is the georeferencing of the BIM models, and IFC can satisfy this aspect. The approach of converting the 3D Cartesian to GCS adopted in this study is done on the 3D STL buildings exported from SketchUp rather than on the model's IFC. Hence, the STL model is converted to the "OSG-36" coordinate system that is broadly utilized in the UK, thereby aligning with the borehole record data used in the Case Study discussed later. SketchUp therefore places the 3D building objects correctly, allowing efficient correlation and integration with the tunnel and geology associated with the rest of the 3D model. This set-up of STL is demonstrated in Figures 6 and 7.

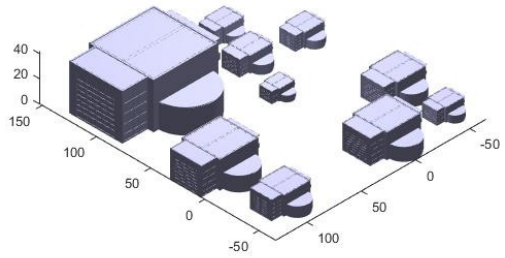

Figure 6. STL buildings in local BIM coordinate system.

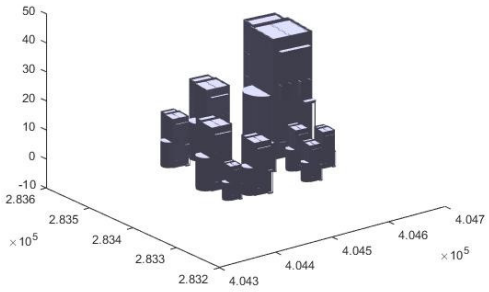

Figure 7. STL buildings transformed to the OSD-36 coordinate system.

3.3. Georeferenced 3D model of the shallow subsurface

The case study is located on the southwestern corner of the campus of the University of Birmingham, UK, approximately 4 km south-west of Birmingham city-centre, with a National British Grid reference of 404420, 283310 (OSG-36).

The part of the campus being considered is shown in Figure 8. This site was chosen for the 3D underground modelling and settlement risk assessment for this study due to the availability of ground investigation data associated with the construction of the new National Buried Infrastructure Facility (NBIF). The ground investigations took place from 2016 to 2017 and consisted of 9 boreholes, the locations of which are shown in Figure 9.

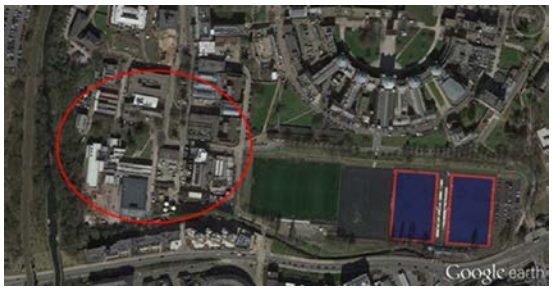

Figure 8. The case study location (satellite image by Google Earth (2018)).

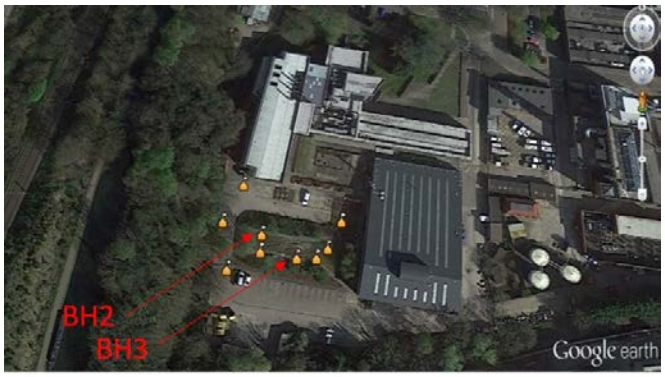

Figure 9. The borehole locations (satellite image by Google Earth (2018)).

The site covers an area of approximately 2.5km^2. The ground investigation confirmed the topsoil of made ground underlying the whole site, with superficial alluvial deposits underneath. The bedrock is Wilmslow Sandstone with a weathered to clay top.

The georeferenced 3D shallow subsurface model comprises 3D geological layering and initially utilized the borehole records data from the ground investigations.

Tables 1 and 2 provide representative data from the borehole logs of BH3 and BH2 (conducted during the site investigations) respectively, these being examples of the information used to produce the 3D geological strata. Their locations in relation to the other seven boreholes drilled as part of the ground investigations are shown in Figure 9. The nine borehole logs, along with geological maps from the British Geological Survey (UKRI NERC, 2018a,b; these are available online and provide geological information of the wider area) constituted the main information used in creating the 3D model of the examined area.

Table 1: Borehole log summary for BH3, adapted from the ground investigations for the site.

Geological Stratum – BH3	**Depth (m)**
Made ground (gravel, red-brick gravel, cobbles with concrete)	0-5.0
Clay (stiff brown sandy)	5.0-6.0
Sandstone (very weak brown / sub-horizontal discontinuities, with a 30mm band of brown sandy clay)	6.0-6.85
Clay (stiff brown locally grey gravelly slightly sandy)	6.85-7.6
Sandstone (very weak brown / horizontal to sub-horizontal discontinuities, with thin mudstone bands)	7.6-20.5 (borehole completed)

Table 2: Borehole log summary for BH2, adapted from the ground investigations for the site.

Geological stratum – BH2	**Depth (m)**
Made ground (brown sand, sandy gravel, red-brick gravel and concrete)	0-3.3
Gravel (dense brown sandy clayey)	3.3-6.3
Clay (stiff brown)	6.3-6.5
Sandstone (very to extremely weak and thinly bedded / horizontal discontinuities, with very thin mudstone bands)	6.5-20.5 (borehole completed)

Triangulated interpolation is then conducted in MATLAB to create the geological layers within the 3D model. This is achieved by modelling the top and bottom surfaces of each layer, utilising its thickness and

subsequently joining them together into a single layer or stratigraphic unit. The boundaries of the geological layers can be adapted by using a standard triangulation algorithm in MATLAB, as it proved to be both feasible and efficient for carrying out geological layering and modelling. In detail, the thickness estimation of the topsoil is carried out by subtracting the available Digital Elevation Model (DEM) data from the boundary depth of the first layer taken from the borehole records.

Due to the lack of open-access DEM data aligning with the study area, the elevation data was processed from Google Earth (Google Inc, 2018) to form a DEM for the area. This was achieved by collecting the elevation data for 200 points across the site from Google Earth Pro (Google Earth, 2018). This proved sufficient for the present study, however other approaches should be considered for other engineering studies depending on their focus and required DEM scales. In addition, to make sure that there were no gaps or overlaps between the geological strata, the bottom surface was set to align with the top surface of the layer beneath. The resulting 3D geology for the site is presented in the Figure 10 and with exploded view in Figure 11.

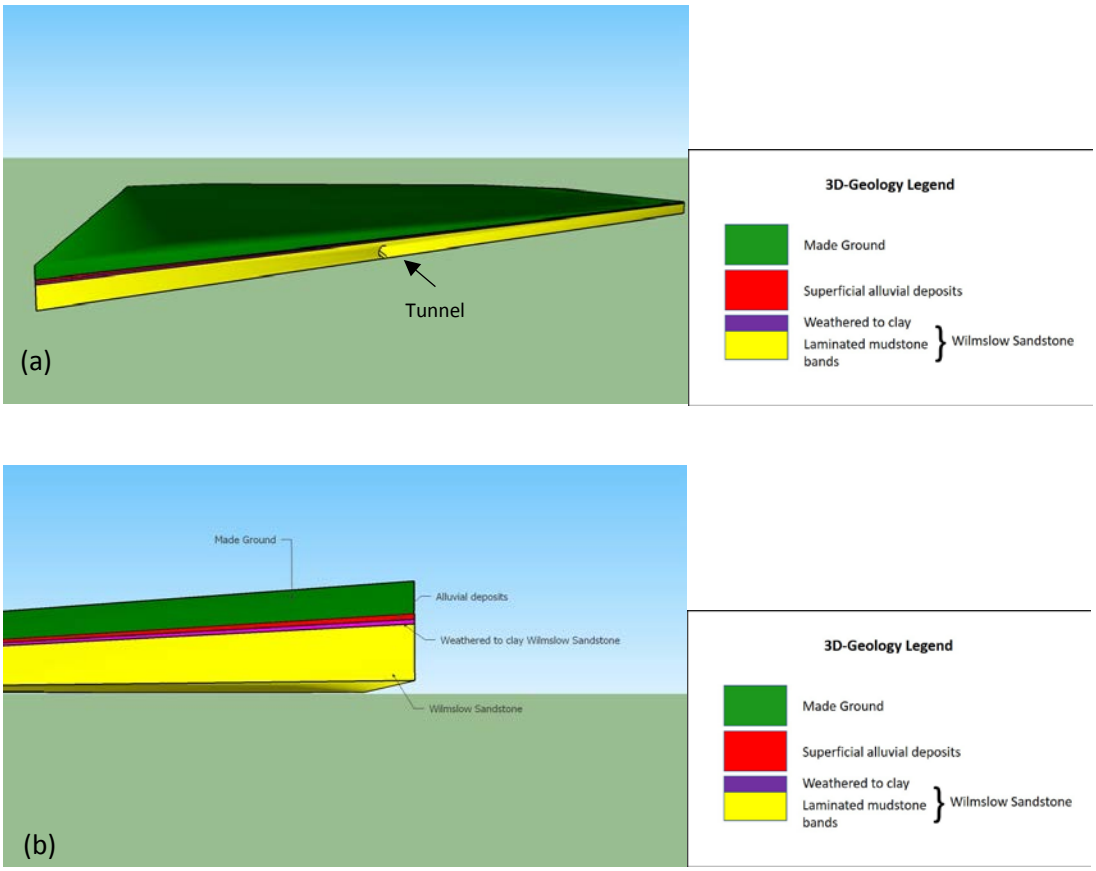

Figure 10. Alternative views (a, b) of the 3D geology.

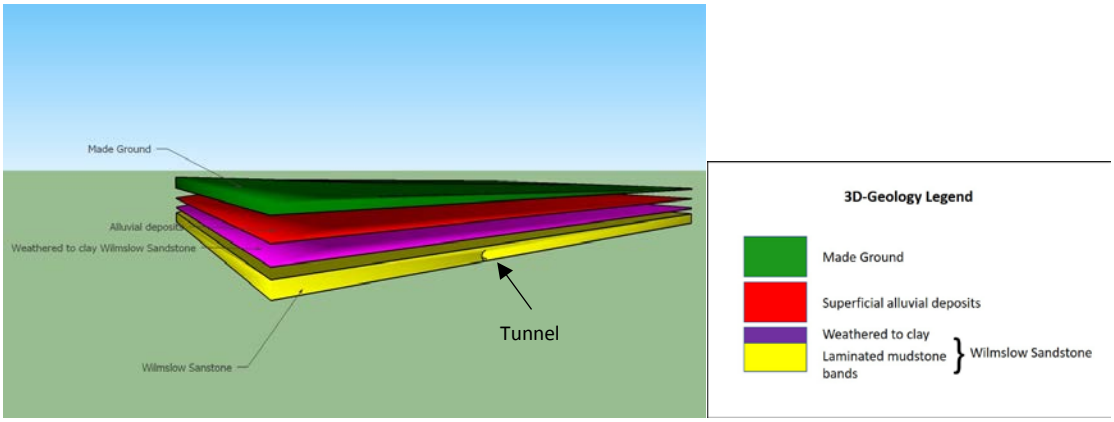

Figure 11. Alternative view of the exploded 3D geology in BIM.

3.4. 3D georeferenced tunnel model

The next stage is to include the 3D tunnel model into the 3D geology model. This is produced by a cylindrical surface triangulation. In this study, a cylindrical surface of a diameter of 12m was adopted at a depth of approximately 20m (100mAOD) for the tunnel's centerline. The proposed methodology utilizes the differential Boolean operation function of MATLAB between the subsurface layer meshing and the tunnel model meshing. Thus, the integrated 3D Ground-Building-Tunnel meshing model was produced and is presented in the Figure 12.

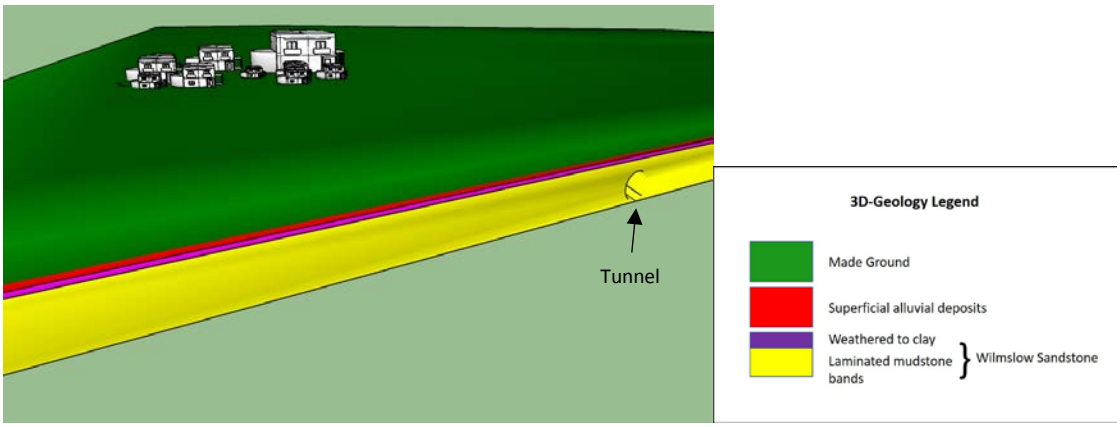

Figure 12. 3D buildings-subsurface-tunnel objects views in BIM.

4. 3D Tunnelling-induced risk assessment results and discussion

As stated previously, there are a number of approaches adopted in the literature for the assessment of building risk due to tunnelling, of which the methodology described below is one. However, it is the principle of its use in a BIM type environment that is being demonstrated in this paper rather than suggesting this is the only (or best) method to adopt. The assessment method involves two Phases:

4.1. Phase 1 Preliminary building damage assessment

Since any 3D building object in the site area is embedded in the integrated building-subsurface-tunnel modelling process, the preliminary Phase 1 building damage assessment procedure as described earlier in the methodology flow chart (Figure 2) was conducted. At this stage the building risk category was estimated using the approach developed by Rankin (1988) and adapted from CIRIA (1996); this is presented in Table 3. The damage classification of each building was produced after extraction of the maximum settlement of the ground underneath each building footprint and the maximum slope (tilt). The maximum slope of each building was estimated from the ratio of the differential settlement between the predicted maximum and minimum settlement within each building footprint divided by the distance between the meshing points of these settlements. This estimation was carried out in MATLAB.

Table 3. Damage classification – typical values, adapted from Rankin (1988), CIRIA (1996) and Chapman (2010).

Risk Category	**Maximum slope of building**	**Maximum settlement of building (mm)**	**Risk description**
1	< 1/500	< 10	Negligible: superficial damage unlikely
2	1/500 to 1/200	10 to 50	Slight: possible superficial damage that is unlikely to have structural significance
3	1/200 to 1/50	50 to 75	Moderate: expected superficial damage and possible structural damage to building, possible damage to relatively rigid pipelines
4	> 1/50	> 75	High: expected structural damage to buildings and rigid pipelines or possible damage to other pipelines

To extract the maximum and minimum settlement falling inside the building footprint, the ground settlement as well as the horizontal movement was derived in 3D by employing Equation (4) in MATLAB and producing settlement susceptibility maps using SketchUp software. From this ground displacement information, two risk based colour maps were produced; one for the ground surface settlement, which extends across the ground surface, and one for the slope of the buildings, which is presented by colours on the faces of each of the investigated buildings.

To demonstrate the proposed methodology, three different locations of the tunnel centreline have been considered: 30m and 10m offset from the first building and beneath the building block. Figures 13-15 present in 3D the impact of tunnelling on the adjacent buildings as the distance to them decreases. It is evident that the proposed 3D visualization approach enhances the multidimensional assessment depictions, thereby providing a better understanding of the risks associated with the different tunnelling options.

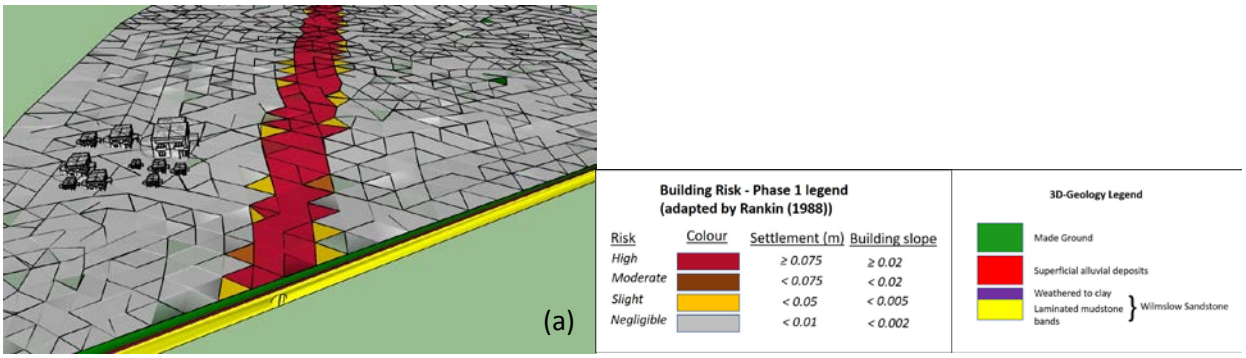

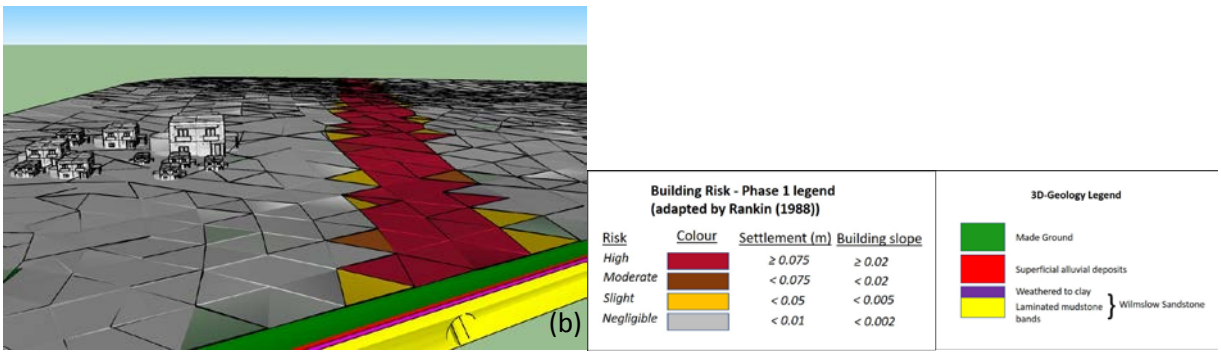

Figure 13. The settlement risk assessment for a tunnel 30m away. (a) Normal view (b) Close view.

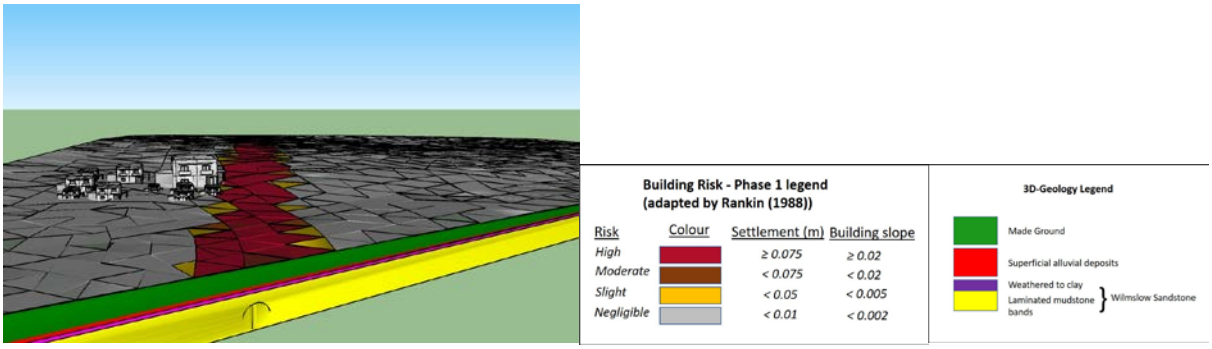

Figure 14. The settlement risk assessment for a tunnel 10m away.

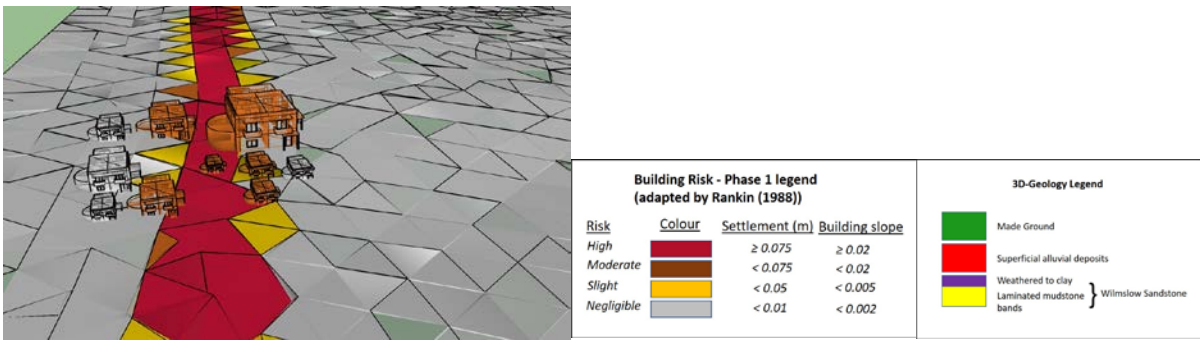

Figure 15. The settlement risk assessment for a tunnel below the buildings.

4.2. Phase 2 Secondary building damage assessment

Those buildings with a rating of “Moderate” or “High” in terms of the preliminary damage assessment in the Phase 1 risk assessment were taken forward into Phase 2. Phase 2 investigates in more detail the likely damage to each building. This could be achieved via empirical, analytical or numerical modelling approaches, however by way of demonstration an empirical based method is shown in this paper. This approach considered the strains associated with “hogging” or “sagging” (settlement trough approach) under the buildings, as indicated in Figure 16.

Equations (5) to (7) show the bending (Σ_b), diagonal (Σ_d) and horizontal (Σ_h) strain (Burland and Wroth, 1974):

$$\frac{\Delta}{B} = \left(\frac{L}{12t} + \frac{3IE}{2tLHG}\right)\varepsilon_b \quad (5)$$

$$\frac{\Delta}{B} = \left(\frac{HL^2G}{18IE} + 1\right)\varepsilon_d \quad (6)$$

$$\varepsilon_h = \frac{\Delta_h}{B_d} \quad (7)$$

where H = Building height; E/G = Relationship between Young's modulus and shear modulus of the building; L = Length of the considered building span; I = Section moment of area of the equivalent beam height of the building at the respective zone (sagging zone: $I=H^3/12$ and hogging zone: $I=H^3/3$); t = Furthest distance from the neutral axis to the edge of the equivalent beam (sagging zone: $t=H/2$, hogging zone: $t=H$); Δ = Maximum relative settlement (deflection) at the considered span; Δ/L = Ratio between the maximum relative settlement at the considered span and the length of this span (deflection ratio); B = Building width.

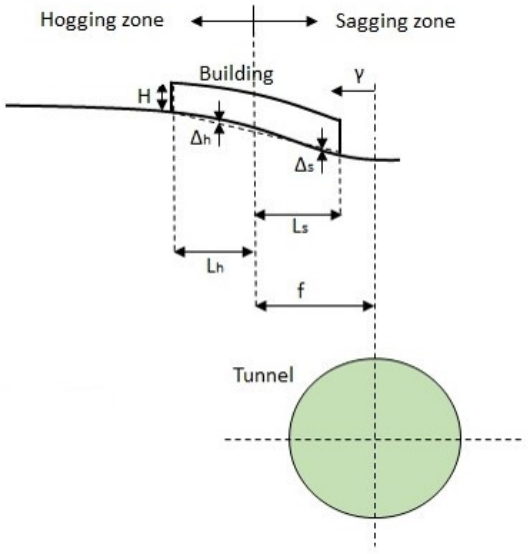

Figure 16. Definitions of "Hogging" and "Sagging" conditions associated with buildings in relation to ground settlement (adapted from O'Reilly and New, 1982; Boscardin and Cording, 1989; Burland, 1995).

In addition, the total bending, diagonal and critical strains based on the 3D building footprint are calculated using Equations (8) to (10) (Boscardin and Cording, 1989; Burland, 1995):

Total bending strain

$$\varepsilon_{bs} = \varepsilon_{b,max} + \varepsilon_h \quad (8)$$

Diagonal strain

$$\varepsilon_{ds} = \varepsilon_h \left(\frac{1-\nu}{2}\right) + \sqrt{\varepsilon_h^2 \left(\frac{1-\nu}{2}\right)^2 + \varepsilon_d^2} \quad (9)$$

Critical strain

$$\varepsilon_{critical} = \max(\varepsilon_{bs}, \varepsilon_{ds}) \quad (10)$$

The critical strain was then correlated to a damage category using Table 4 developed by Boscardin and Cording (1989) and Burland (1995).

Table 4: Tunnelling-induced building damage categories adapted by Burland et al. (1977), Boscardin and Cording (1989) and Burland (1995).

Category of damage	**Normal degree of severity**	**Critical strain (Limiting Tensile Strain)**
1	Negligible	0-0.05
2	Very slight	0.05-0.075
3	Slight	0.075-0.15
4	Moderate	0.15-0.3
5	Severe to very severe	> 0.3

To conduct the Phase 2 building damage assessment there were various parameters that needed to be assessed in Equations (5) to (10) related to the geometric aspects of the building being assessed. For example, in this study it was assumed that for all the buildings the ratio E/G is equal to 2.6 (masonry structure) (Boscardin and Cording, 1989). All buildings investigated are two-storey masonry structures, ranging from 100 to 300 m^2 in gross plan area. Internally they comprise four rooms on each floor, including two small outer balconies and a large internal balcony, which is surrounded by glass openings up to the ceiling. All buildings are supported on a strip foundation. These geometric features for each building being assessed can be obtained from the georeferenced STL building model and the resulting triangulated mesh as shown in Figure 17 and described in the following points:

1. A horizontal plane through the building, together with two vertical planes were chosen to pass through the centroid of the building. An adequate number of intersection points with their georeferenced 3D coordinates were extracted along the building shape envelope.

2. The maximum distances in relation to the horizontal section plane provided both the width and the length of each building being assessed, while the maximum distance in the vertical plane provided the height of each building.

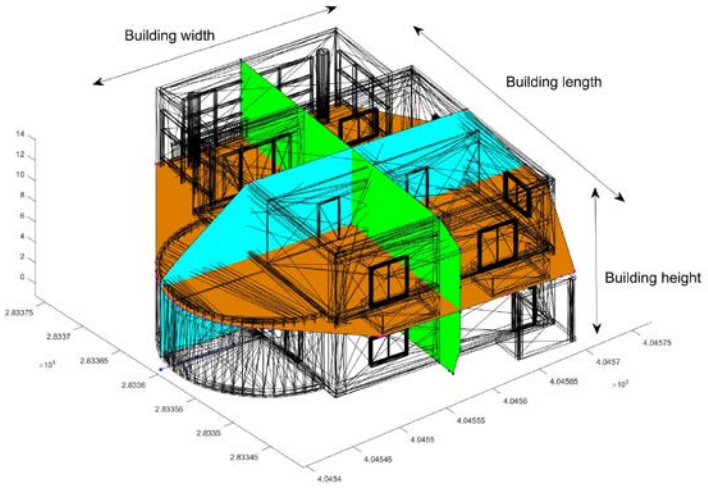

Figure 17. The triangulated mesh approach used in this study, and how the various building parameters were estimated for the Phase 2 risk assessment. Orange: Horizontal plane. Cyan and Green: Vertical planes.

After the evaluation of critical strain from Equation (10) for each building, a colourmap can be adopted for the background colour of the building faces. In addition, the settlement curve below every assessed building in that direction can also be visualized below each building.

The map of buildings used in the current study is shown in Figure 18. Figures 19-22 present examples of the Phase 2 risk assessment, with the settlement trough demonstrated as the blue curve below the buildings in comparison with the horizontal level (green line). For the same figures, the buildings used were selected in order to provide a thorough view of the assessment by indicating different risk. The rest

of the coloured dots in the demonstrations show the section planes. More specifically, the blue, red and pink/purple dots define the outer shape of each investigated building, and they are represented by planes passing through the centroid of the building, being parallel to the length (vertical plane of Figure 17 in green), the width (vertical plane of Figure 17 in cyan) and the footprint plan area (horizontal plane of Figure 17 in orange) of the building, respectively.

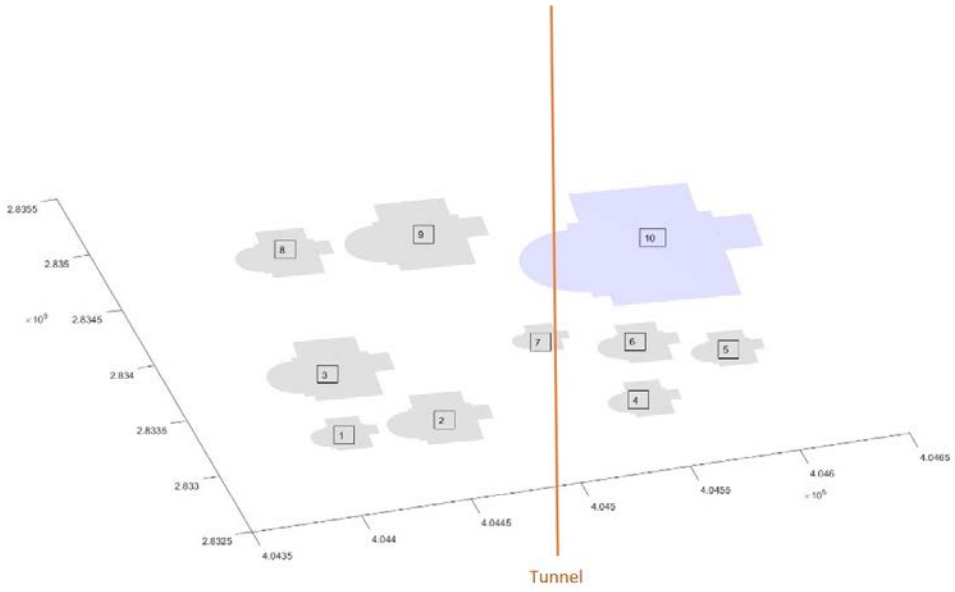

Figure 18. The map of the building footprints and the tunnel's centreline.

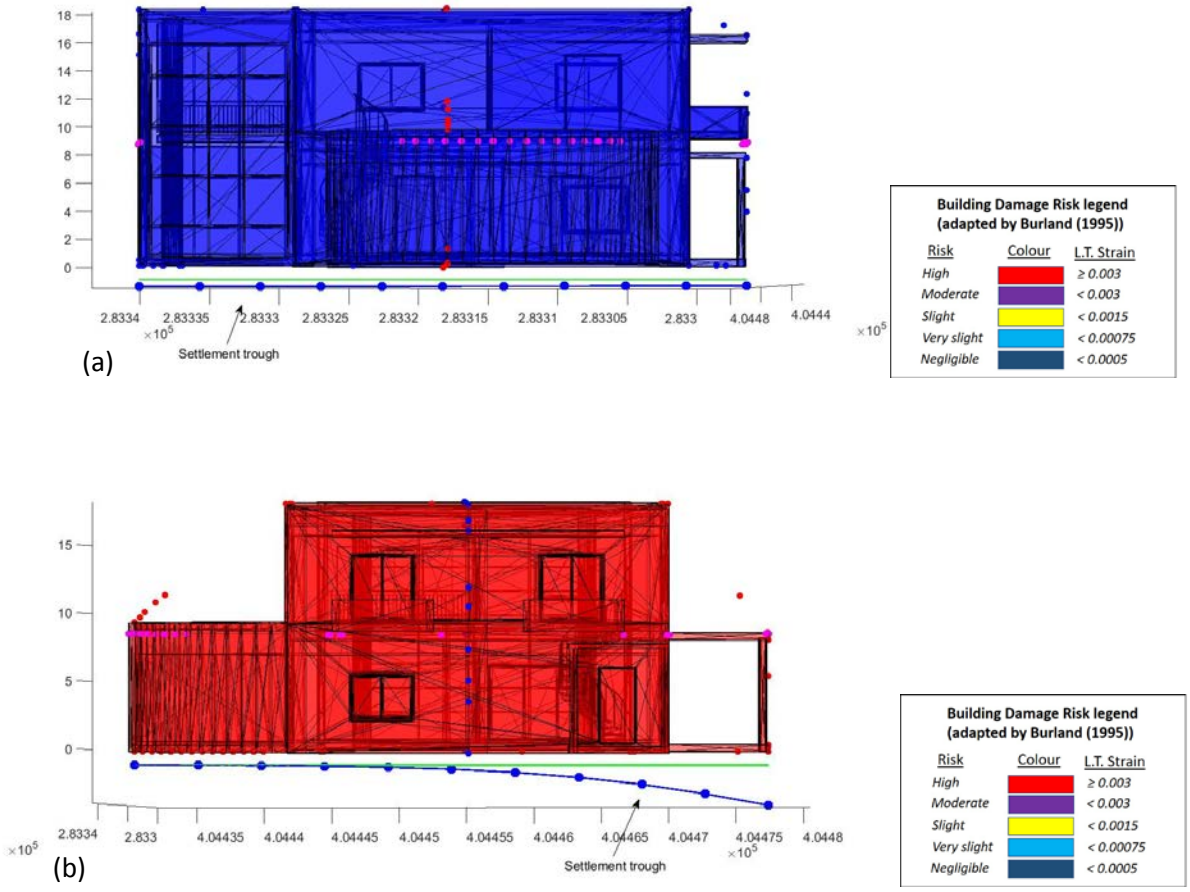

Figure 19. Phase 2 assessment and damage risk level for the Building 2, (a) along the longest dimension and (b) along the vertical dimension.

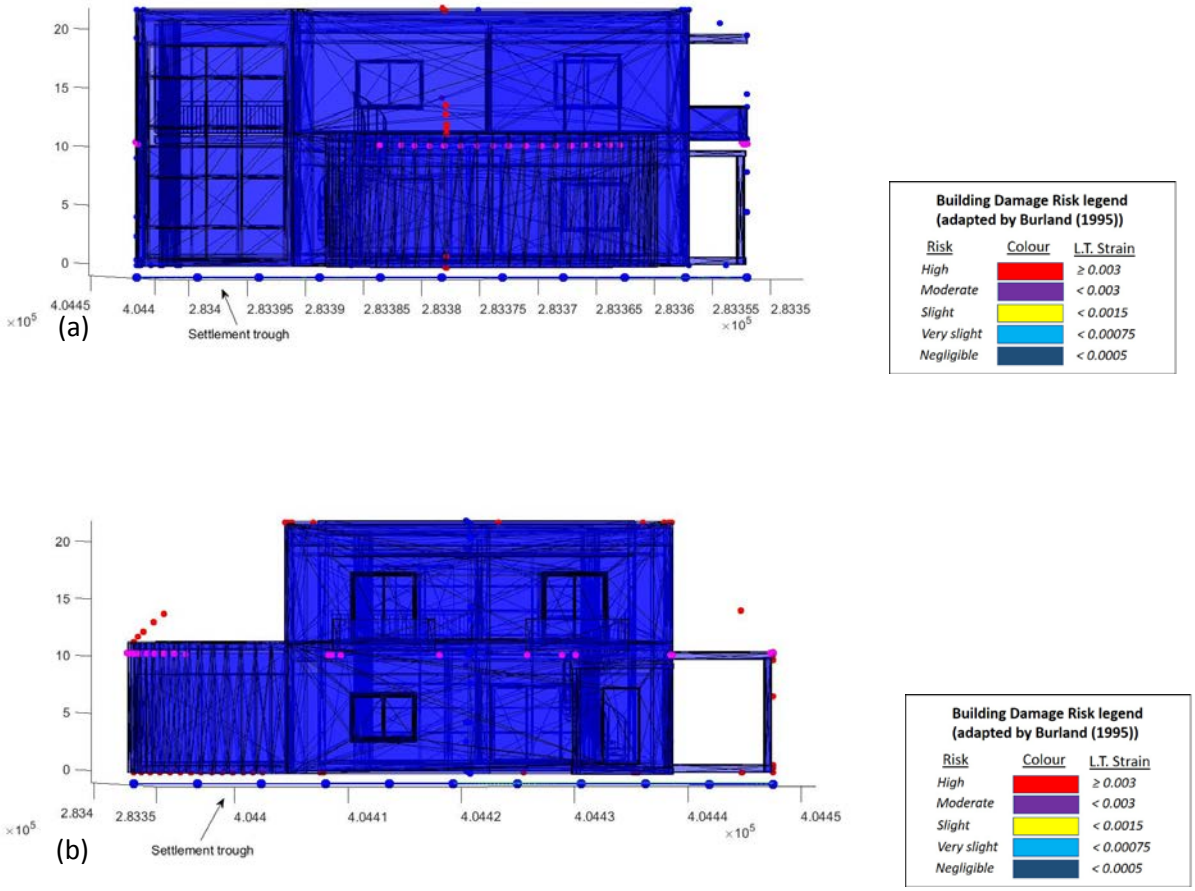

Figure 20. Phase 2 assessment and damage risk level for the Building 3, (a) along the longest dimension and (b) along the vertical dimension.

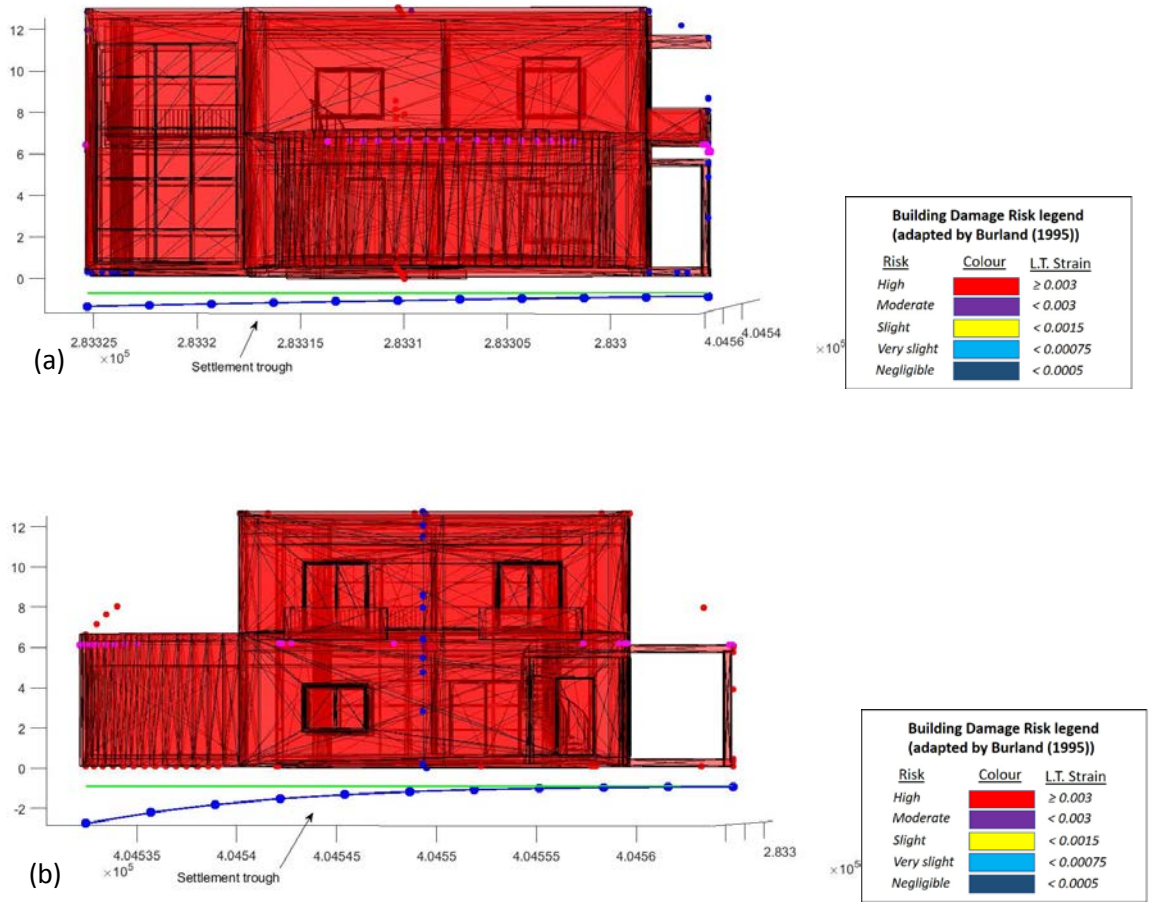

Figure 21. Phase 2 assessment and damage risk level for the Building 4, (a) along the longest dimension and (b) along the vertical dimension.

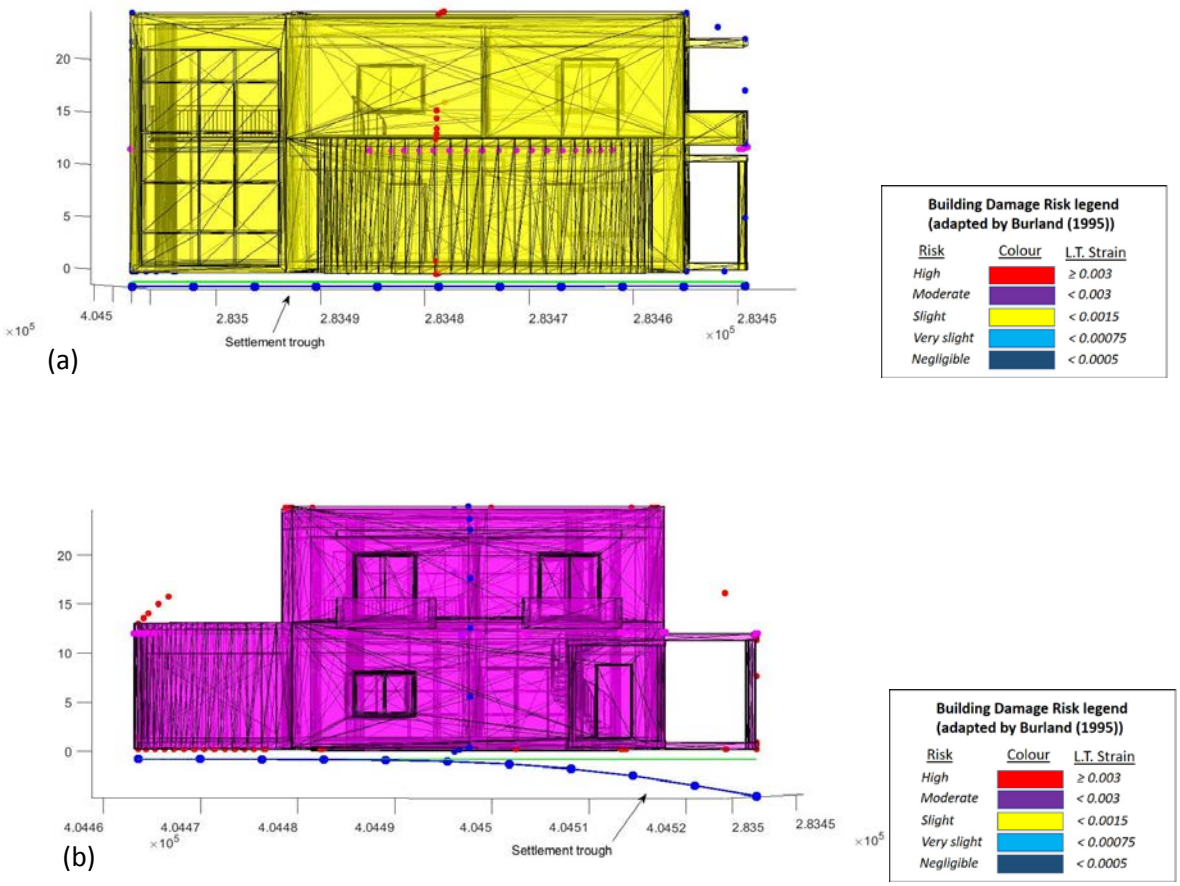

Figure 22. Phase 2 assessment and damage risk level for the Building 9, (a) along the longest dimension and (b) along the vertical dimension.

As demonstrated in the previous analysis, the methods proposed in this paper can provide a unique way of integrating both the building-related BIM models with the geological information in a dynamic way that allows users to assess the effects of new construction activities on existing infrastructures. In the case of this paper, this has involved a new tunnel construction affecting existing buildings. The ability to integrate calculations (this can be via empirical, analytical or numerical modelling methods) and visualisations within a dynamic BIM environment is a unique feature of the presented modelling

approach. Although this has been demonstrated using a relatively simple example, it can be extended to provide a powerful tool for decision makers.

5. Conclusions

This paper has presented an integrated 3D BIM-geology interaction methodology that can include the effects of new infrastructure construction on the surrounding environment. This methodology has made use of a combination of MATLAB tools, the 3D visualization capabilities of the Sketchup design software and the conversion procedures from BIM to IFC to STL models and vice versa.

The example used in this paper to demonstrate the proposed approach has involved a new tunnel construction and the associated damage assessment for the buildings in the vicinity of this construction. This approach begins with the extraction of basic engineering parameters (e.g. building geometries) adopted in the BIM framework to generate the corresponding settlement input data to the integrated model.

It has been also shown from the outcomes of the proposed methodology that, while there has been a growing interest in the other domains of the AEC industry for the use of the IFC, there is certainly potential in geotechnics.

The access to detailed interaction information and powerful visualisations could provide a powerful decision-making tool that is able to assess a number of different options in the same modelling environment. In the case demonstrated in this paper, i.e. the effects of a new tunnel on existing buildings, it can assist route decisions and the effects of these decisions in terms of building risk assessment. The proposed framework taking into account the interactions between the 3D BIM structural models and the associated geological interactions, although posing a number of challenges, also has the potential to be extended to city or regional scales, due to the efficient nature of the proposed approach.

Acknowledgements

The authors gratefully acknowledge the financial support of the UK Engineering and Physical Sciences Research Council (EPSRC) under grant number EP/N010523/1 (Balancing the impact of City Infrastructure Engineering on Natural Systems using Robots), to which this PhD project was linked, and the first author gratefully acknowledges the financial support of the University of Birmingham.

References

3D systems, 2018. STL File (website: https://uk.3dsystems.com/) [Accessed 5 March 2018].

Attewell, P.B. and Woodman, J.P., 1982. Predicting the dynamics of ground settlement and its deriving caused by tunnelling in soil. *Ground Engineering 15* (7), PP.13–22.

Attewell, P.B, Yeats, J, and Selby, A.R, 1986. Soil Movements Induced by Tunneling and Their Effects on Pipelines and Structures. Glasgow: Blackie.

Autodesk Inc., 2018. Revit (website: https://www.autodesk.co.uk) [Accessed 10 March 2018]

Borrmann, A., Kolbe, T., Donaubauer, A., Steuer, H., Jubierre, J. and Flurl, M., 2014. Multi-Scale Geometric-Semantic Modeling of Shield Tunnels for GIS and BIM Applications. *Computer-Aided Civil and Infrastructure Engineering*, *30* (4), pp.263-281.

Boscardin, M. D. and Cording, E. J., 1989. Building response to excavation–induced settlement. *Journal of Geotechnical Engineering 115*(1), 1–21.

buildingSMART, 2017. Industry Foundation Classes Edition 3 (website: http://www.buildingsmart.org) [Accesed 20 March 2017].

Burland, J. B., 1995. Assessment of risk of damage to buildings due to tunnelling and excavation. Invited Special Lecture. *In: 1st Int. Conf. on Earthquake Geotech. Engineering, IS Tokyo '95*.

Burland, J. B. and Wroth, C. P., 1974. Settlement of buildings and associated damage. In Settlement of structures, pp. 611–654. London: Pentech Pr.

Burland, J. B., Standing, J. R., Jardine, F. M., 2001. Building response to tunnelling - Case studies from construction of the Jubilee Line Extension, Volume 1: Projects and Methods. London: T. Telford.

Burland, J.B., Broms, J.B. and de Mello, V.F.B., 1977. Behavior of foundations and structures on soft ground. *Proceedings of the 9th International Conference on Soil Mechanics and Foundation Engineering (SMFE), Tokyo, Japan, July 10- 15, 1977,* pp.495-546.

Chapman, D.N., 2010. Introduction to tunnel construction / David N. Chapman, Nicole, and Alfred Stärk. Taylor & Francis, New York.

Chiu, W.K. and Tan, S.T., 2000. Multiple material objects: from CAD representation to data format for rapid prototyping. *Computer-aided design*, *32*(12), pp.707-717.

CIRIA, 1996. Prediction and effects of ground movements caused by tunnelling in soft ground beneath urban areas. Construction Industry Research and Information Association (CIRIA). Project Report 30.

Cording, E.J. and Hansmire, W.H., 1975. Displacements around soft ground tunnels. *Proceedings of the 5th Pan-American Conference on Soil Mechanics and Foundation Engineering, Buenos Aires, Argentina, October 27-31, 1975,* pp.571-633.

Eastman, C., Teicholz, P., Sacks, R. and Liston, K., 2011. BIM Handbook (2nd Edition) A Guide to Building Information Modeling for Owners, Managers, Designers, Engineers and Contractors, John Wiley & Sons, New Jersey

Google Earth, 2018. Birmingham, UK; (from website: http://www.google.com/earth/index.html) [Viewed 15 March 2018].

Google Earth, 2018. Birmingham, UK; (from website: http://www.google.com/earth/index.html) [Viewed 18 March 2018].

Google Inc., 2015. Google Earth Pro (website: https://earth.google.com/download-earth.html) [Accessed 15 June 2017].

Graphisoft Inc., 2018. Archicad 22 (http://www.graphisoft.com/archicad/) [Accessed 15 January 2018].

Hunt, D., Makana, L., Jefferson, I. and Rogers, C.D.F., 2016. Liveable cities and urban underground space. *Tunnelling and Underground Space Technology, 55*, pp.8-20.

Imseeh, W.H. and Alshibli, K.A., 2018. 3D finite element modelling of force transmission and particle fracture of sand. *Computers and Geotechnics Volume 94*, Pages 184-195.

Kessler, H., Wood, B., Morin, G., Gakis, A., McArdle, G., Rabson, O., Fitzgerald, R. and Dearden, R., 2015. Building Information Modelling (BIM) – A Route for Geological Models to Have Real World Impact. Special Report. AER/AGS, pp.13-18.

Kim, S., Kim, J., Jung, J. and Heo, J., 2015. Development of a 3D Underground Cadastral System with Indoor Mapping for As-Built BIM: The Case Study of Gangnam Subway Station in Korea. *Sensors*, *15*(12), pp.30870-30893.

Loganathan, N. and Poulos, H., 1998. Analytical Prediction for Tunneling-Induced Ground Movements in Clays. *Journal of Geotechnical and Geoenvironmental Engineering, 124*(9), pp.846-856.

Mair, R. J., 1993. The unwin memorial lecture 1992: Developments in geotechnical engineering research: application to tunnels and deep excavations. *Proc. Instn. Civ. Engrs. Civil Engineering, 97*, pp. 27-41.

Mair, R. J., Taylor, R. N. and Burland, J. B., 1996. Prediction of ground movements and assesment of risk of building damage due to bored tunnelling. *In Geotechnical aspects of underground construction in soft ground,* pp. 713–718. Rotterdam: Balkema.

Mathworks Inc., 2016. Matlab R2016a (https://uk.mathworks.com/products/matlab.html) [Accessed 12 December 2016].

O'Reilly, M.P. and New, B.M., 1982. Settlements above tunnels in the United Kingdom – their magnitude and prediction. *Tunnelling'82*. The Institution of Mining and Metallurgy, London, pp. 55–64.

Peck, R.B., 1969. Deep excavations and tunnelling in soft ground. *In: Proceedings of the 7th International Conference on Soil Mechanics and Foundation Engineering, State of the Art Volume, vol. 3. Mexican Society of Soil Mechanics, Mexico,* pp. 225–290.

Price, S., Ford, J., Campbell, S. and Jefferson, I., 2016. Urban Futures: the sustainable management of the ground beneath cities. *Geological Society, London, Engineering Geology Special Publications*, *27*(1), pp.19-33.

Qu, X., and Stucker, B., 2003. A 3D surface offset method for STL-format models, *Rapid Prototyping Journal, Vol. 9* Issue: 3, pp.133-141.

Rankin, W., 1988. Ground movements resulting from urban tunnelling: predictions and effects. Geological Society, London, *Engineering Geology Special Publications*, *5*(1), pp.79-92.

Rogers, C.D.F., 2009. Substructures, underground space and sustainable urban environments. Geol. Soc., London, *Eng. Geol. Spec. Publ. 22* (1), 177–188.

Sagaseta, C., 1987. Analysis of undrained soil deformation due to ground loss. *Geotechnique*, London, England, 37, 301-320.

Schindler, S., Hegemann, F., Koch, C., König, M. and Mark, P., 2016. Radar interferometry based settlement monitoring in tunnelling: Visualisation and accuracy analyses. *Visualization in Engineering* pp.4-7.

Silva, M., Salvado, F., Couto, P. and Azevedo, Á., 201. Roadmap Proposal for Implementing Building Information Modelling (BIM) in Portugal. *OJCE*, *06*(03), pp.475-481.

Steel, J., Drogemuller, R. and Toth, B., 2012. Model interoperability in building information modelling. *Softw Syst Model* (11) pp. 99–109.

SUPodium, 2018. SUPlugins (from website: http://www.SUplugins.com/ifc2skp.php) [viewed on 3 June 2018].

Tawelian, L. and Mickovski, S., 2016. The Implementation of Geotechnical Data into the BIM Process. Procedia Engineering, 143, pp.734-741.

Trimble Inc., 2016. Sketchup Pro 2016. (https://www.sketchup.com/) [Accessed 3 November 2016]

UKRI NERC, 2018a. BGS Geoindex. From website: https://www.bgs.ac.uk/geoindex/ [Accessed 10.06.2018].

UKRI NERC, 2018b. BGS Geology of Britain viewer. From website: https://www.bgs.ac.uk/discoveringGeology/geologyOfBritain/viewer.html [Accessed 10.06.2018].

Verruijt, A., and Booker, J. R., 1996. Surface settlements due to deformation of a tunnel in an elastic half plane." *Geotechnique*, London, England, 46(4), 753-756.